Journal of the Korean Ceramic Society (2020) 57:557–569
https://doi.org/10.1007/s43207-020-00061-w

ORIGINAL ARTICLE

Effect of magnetic particles adding into nanostructured hydroxyapatite–alginate composites for orthopedics

L. F. Sukhodub[1] · L. B. Sukhodub[1] · A. D. Pogrebnjak[1,2] · Amanzhol Turlybekuly[2] · A. Kistaubayeva[3] · I. Savitskaya[3] · D. Shokatayeva[3]

Received: 10 February 2020 / Revised: 15 May 2020 / Accepted: 20 May 2020 / Published online: 15 June 2020

Abstract
The composite materials based on hydroxyapatite (HA), sodium alginate (Alg)–magnetite (Fe_3O_4) were synthesized by the "wet chemistry method" under the influence of microwave irradiation and ultrasound. The biomagnetic samples were investigated by XRD, RFA, SEM, TEM and colorimetric assay methods. The cytotoxicity was assessed on fibroblasts cultures. It was found that the synthesis of Fe_3O_4 particles in the presence of Alg macromolecules leads to magnetite nanoparticles' average size decreasing (up to 8 nm). The presence of samples with applied magnetite content (1% of HA) in a nutrient medium did not influence on cells viability. It was shown that the hydrogels were more conducive to cells survival and provide a greater degree of cell proliferation in comparison with beads. It was concluded that Fe_3O_4-loaded hydroxyapatite–alginate composites are characterized by good adhesive ability of the fibroblast cells and its bioactivity.

Keywords Biomagnetic composites · Hydroxyapatite–alginate composites · Bioactivity and cytotoxicity

1 Introduction

Bone defects and fractures as a result of industrial, sports and war injuries, pathologies and resorption are a major problem of orthopedics, maxillofacial surgery and rehabilitation medicine. One approach to solve this problem is bone tissue engineering. Therefore, extensive research work was devoted to the development of optimal bioactive materials, which should have a highly micro-porous and interconnected three-dimensional structure, as well as a function to simulate the physico-chemical properties of native bone. Materials for bone regeneration are designed with characteristics necessary for new bone growth, i.e., osteoconductivity, osteogenecity, and osteoinductivity [1].

Hydroxyapatite has broad area of application as a biocompatible material in medicine, since it is the main component of bone tissue [2]. As an inorganic component of bone, HA nanoparticles have excellent biocompatibility, especially good osteoconductivity, which have been widely used in medicine and dentistry [3–5]. Composites consisting of polymer–ceramics best mimic the natural functions of bone. Natural-derived polysaccharides such as chitin, chitosan, alginate, carrageenan and chondroitin sulfate are widely used versatile biomaterials for bone tissue engineering applications. Among the natural polysaccharides, alginate is widely used as a biomaterial for bone tissue engineering. Alginate, an anionic polymer owing enormous biomedical applications, is gaining importance, particularly in bone tissue engineering, due to its biocompatibility and gel forming properties [6]. The alginate composites show enhanced biochemical significance in terms of porosity, mechanical strength, cell adhesion, biocompatibility, cell proliferation, alkaline phosphatase increase, excellent mineralization and osteogenic differentiation [7, 8]. Hence, alginate-based composite biomaterials will be promising for bone tissue.

Magnetite (Fe_3O_4) is the most common iron oxide used in biomedicine due to its low toxicity, relative ease of functionalization and high magnetization at room temperature [9, 10]. Magnetic materials can be introduced into the scaffolds, to promote bone formation [11]. The biomedical application of magnetic nanoparticles (MNPs) have increased in recent decades [12–14]. Iron ions in MNPs containing iron

✉ Amanzhol Turlybekuly
aturlybekuly@gmail.com

[1] Sumy State University, Sumy, Ukraine

[2] D. Serikbayev East Kazakhstan State Technical University, Oskemen, Kazakhstan

[3] Al-Farabi Kazakh National University, Almaty, Kazakhstan

and iron oxides are added to iron deposits into the body after metabolism, and finally included by red blood cells or hemoglobin [15].

There are several key areas for the use of MNPs in medicine. First, MNPs are used in tissue engineering as scaffold for bone regeneration [16, 17]. Therefore, MNPs acted as a drug carrier for effective controlling the delivery and release of drug to a lesion site [17, 18]. The use of bioceramic scaffolds for a targeted drug release significantly improves the treatment efficiency, especially for a disease such as cancer [19, 20]. The third use of MNPs is a clinical medical diagnosis. They may likewise be used in non-invasive diagnostic applications such as magnetic resonance imaging, where the MNPs act as a contrast material due to the local modification of magnetic fields, electric field gradients, and radio waves depending on the employed imaging type [19–24]. Moreover MNPs has practical application in relative cancer treatment [25, 26]. Thus, nanostructured ferromagnetic materials and MNPs are quite well used in medicine. The hydroxyapatite–alginate (HA–Alg) combination can be considered as a physical model of the second-level structure of bone tissue in its 8-level hierarchy [27]. The magnetic component gives the HA–Alg composite magnetic properties and possibility of use in the bone cancer treatment by hyperthermia [28]. We have developed several methods for producing magnetite granules in a polysaccharide shell [29]. Also, we have developed several methods for producing magnetite granules in a polysaccharide shell [29].

In this work, magnetite nanoparticles were synthesized in the presence of natural alginate polymer and then, under the influence of ultrasound, are distributed in alginate macromolecules- and nanostructured hydroxyapatite nanoparticles-containing composite. The obtained biomagnetic composites are presented in the form of a hydrogel and beads, and may be promising in surgery as bone defects' filler.

2 Materials and methods

2.1 Materials

The composite material was synthesized from following chemicals (manufactured by Merck): calcium nitrate tetrahydrate (Ca $(NO_3)_2{\cdot}4H_2O$), ammonium hydrogen phosphate ($(NH_4)_2HPO_4$), sodium hydroxide (NaOH), ferrum sulfate ($FeSO_4{\cdot}7H_2O$), ferrum chloride ($FeCl_3{\cdot}6H_2O$), calcium chloride $CaCl_2$; sodium alginate (Alg) (E401, M.M. 15 kDa, Shanghai Chemical Company Ltd, China). All reagents were of analytical grade.

2.2 Composite preparation

2.2.1 HA (hydrogel)

The HA hydrogel synthesis method is described in [30–33] in detail. Briefly, the HA was synthesized from 50 ml of $Ca(NO_3)_2{\cdot}4H_2O$ (0.5 M) and 50 ml of $(NH_4)_2HPO_4$ (0.3 M). Ammonium hydrophosphate and calcium tetrahydrate were mixed by adding first one dropwise. The ammonia solution was added to get pH of 10.5. The result solution was treated at consumer microwave (MW) oven Samsung M1712NR for 3 min. After MW treatment, the product was cooled and precipitated at room temperature.

2.2.2 Nanostructured magnetite Fe_3O_4 (powder)

Magnetite powder Fe_3O_4 was performed by chemical precipitation method according to the following reaction:

$$2FeCl_3 \cdot 6H_2O + FeSO_4 \cdot 7H_2O + 8NaOH \rightarrow Fe_3O_4 + 6NaCl + Na_2SO_4 + 23H_2O.$$

At the first stage, 5 ml of a 2% aqueous sodium alginate solution was prepared; the pH value of 10 was achieved by adding 18% NaOH solution. 10 ml of 0.4-M $FeCl_3{\cdot}6H_2O$ was added to the alkaline alginate solution, followed by sonication. After the subsequent addition of 10 ml of 0.4-M $FeSO_4{\cdot}7H_2O$, the mixture was kept at 80 °C for 10 min. The settling precipitate was washed with distilled water to neutral pH. After drying, nanostructured magnetite powder was obtained with a final components ratio Fe_3O_4:Alg = 10:1

2.2.3 HA–Fe_3O_4 (hydrogel)

0.11 g of Fe_3O_4 powder (2.2.2) was gradually added to 8.00 g of HA hydrogel (p.2.2.1) and treated with ultrasound of low (90 W) power. Thus, the magnetite content was 1% of HA (calculated on the weight of dry powders). The samples are called as HA–Fe_3O_4 (hydrogel).

2.2.4 HA–Fe_3O_4–Alg (beads)

HA–Fe_3O_4 hydrogel (p.2.2.3) was added to 2% alginate solution in a weight ratio of HA–Fe_3O_4:Alg = 1:1 and mixed with ultrasound for 12 min. The composite material in the form of beads (further named HA–Fe_3O_4–Alg) was obtained by dispersing HA-Fe_3O_4:Alg suspension in a 0.125-M calcium chloride solution. After 25 min of exposition, the beads were filtered, washed with distilled water until neutral reaction and dried.

2.3 Analytical methods

2.3.1 XRD analysis

The samples X-ray diffraction (XRD) studies were performed by Shimadzu XRD-6000 diffractometer with Cu-Kα radiation. The JCPDS (Joint Committee on Powder Diffraction Standards) card catalog was used for crystal phases identification.

2.3.2 Determination of Ca/P molar ratio

The X-ray fluorescence spectrometer ElvaX Light SDD (RFA) was used for Ca/P ratio determination. The samples were powdered and put into cylindrical cuvette. The measurements were carried out in a helium inert atmosphere by gas blown.

2.3.3 TEM study

The thin morphology was observed by transmission electron microscope (TEM; PEM-125K, SELMI, Sumy, Ukraine). The accelerating voltage was 90 kV.

2.3.4 SEM study

Microphotographs of the surface of the samples were made in the secondary electron mode with an accelerating voltage $U_{ac} = 20$ kV and a beam current of 1–10 A on JSM-6390LV scanning electron microscope with EDAX microanalysis system.

2.3.5 Cytotoxicity and bioactivity study

The cytotoxicity of the HA–Fe_3O_4 hydrogel and HA–Fe_3O_4–Alg beads was investigated using cell cultures of mouse fibroblasts.

2.3.6 MTT assay

Direct cytotoxicity of materials was assessed by the efficiency of cell attachment on samples. To remove unattached cells after 48 h of cultivation, the films were washed with sodium phosphate buffer. The adherent cells number was evaluated by MTT method.

It should be noted that MTT analysis is one of the dependable and sensitive indicators used for cellular metabolic activity. This analysis is based on the MTT reduction, which is a water-soluble yellow tetrazolium dye. The NIH-3T3 cells were maintained at a concentration equals to 5×10^4 cells per well and by addition in 96-well plates separately (Falcon BD, USA) and Dulbecco's Modified Eagle Medium (DMEM-150 µl) was also added to these wells for cell growth. Then, fibroblasts cells were washed with the medium that is serum free (100 µl) twice and starved for 1 h at 37 °C. When the process of starvation is passed, the NIH-3T3 fibroblast cells were treated with different concentrations of HA–Fe_3O_4–Alg composites (200 µg/ml) for the incubation period of 24 and 48 h. The control one was maintained without adding HA–Fe_3O_4–Alg. The medium was aspirated after each period of experiment finished. The serum-free medium containing 0.45 mg/ml of MTT (3-[4,5-dimethylthiazol-2-yl] 2,5-diphenyl tetrazolium bromide) reagent was added and incubated for 4 h at 37 °C in CO_2 incubator. Thus, these determinations were performed with the usage of triplicates each time.

The medium with MTT was removed and the NIH-3T3 cells were washed with the solution of phosphate buffer (PBS-200 µl) for elimination non-reacted MTT reagent and also HA–Fe_3O_4–Alg. The formazan crystals that were formed and dissolved by addition of 99% DMSO (100 µl) and 0.6% of glacial acetic were mixed thoroughly via pipetting up and down. Purple blue formazan was measured in a microplate reader at 570 nm (Biotek PowerWave 340, USA) by the spectrophotometrical absorbance. The cell viability was determined with a help of Graph pad prism 5 software. The observance of viable NIH-3T3 cells was done by the usage of inverted phase contrast microscopy.

The percentage of cell viability was evaluated by Eq. (1):

$$\text{Percentage of cell viability} = \text{Sample OD/Control OD} \times 100\%. \quad (1)$$

Adhesion, spreading and subsequent cell proliferation were accessed after 3- and 5-day cultivation (fluorescent microscope Zeiss AxioVert 25, Germany). The micrographs of cells were obtained after 5 days of cultivation. For staining the actin filaments of the MC3T3-E1 cytoskeleton cells (green), a phalloidin-labeled Alexa Fluor® 488 (1:20, Invitrogen, USA) was used; the cell nuclei (blue) were stained with 4-6-diamidino-2-phenylindole (DAPI, Invitrogen, USA). Fluorophores, phalloidin-labeled Alexa Fluor® 488 and DAPI were excited at a wavelength of 488 nm using a 505–530-nm bandpass filter and at a wavelength of 543 nm using a 560-nm long-wavelength transmission filter, respectively.

2.3.7 Statistical analysis

Each biological experiment involves 10 samples of each type of material and 3 control cultures. The mean values and 95% confidence interval were calculated for five such experiments. The reliability of the obtained data was evaluated by the U-criterion.

3 Results and discussion

3.1 The morphology characterization

The morphology of HA–Alg composite is illustrated in Fig. 1. The HA is embedded to an alginate matrix by lamellae formation (Fig. 1a mentioned by red circles). The results of elemental analysis are shown in Fig. 2 and Table 1. Lamellas of HA are clearly visible in Fig. 2a. The EDAX spectrum is clear; the peaks of elements are identifiable. The distribution of elements is uniform; quantity deviation does not exceed 5%.

The HA–Fe_3O_4 hydrogel's microstructure study is shown in Fig. 3. It can be seen that magnetite particles are well integrated into hydrogel composition. The magnetite particles' sizes do not exceed 10–15 µm, Fig. 3a, b.

Figure 4a shows an image of the HA section with Fe_3O_4 particles, where the sample composition was analyzed. As

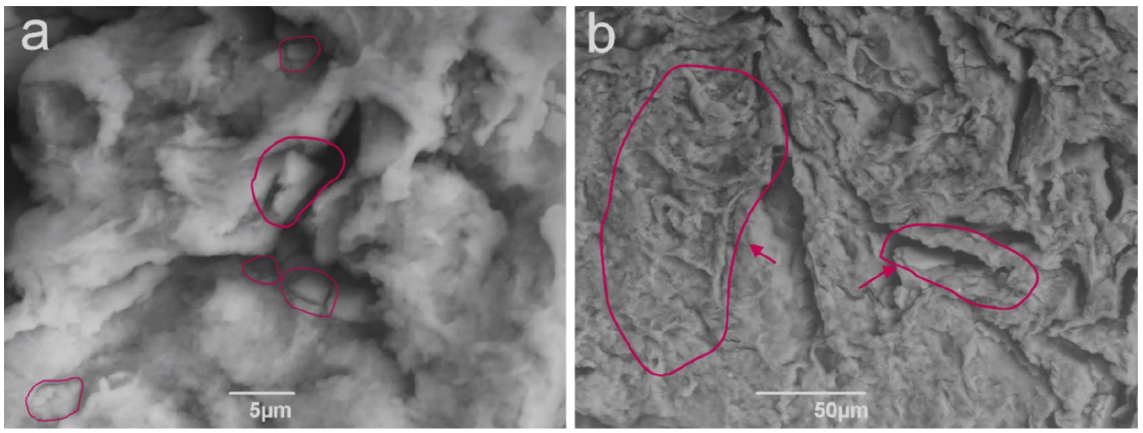

Fig. 1 The SEM image of HA–Alg composite. **a** Magnification × 3000; **b** × 500

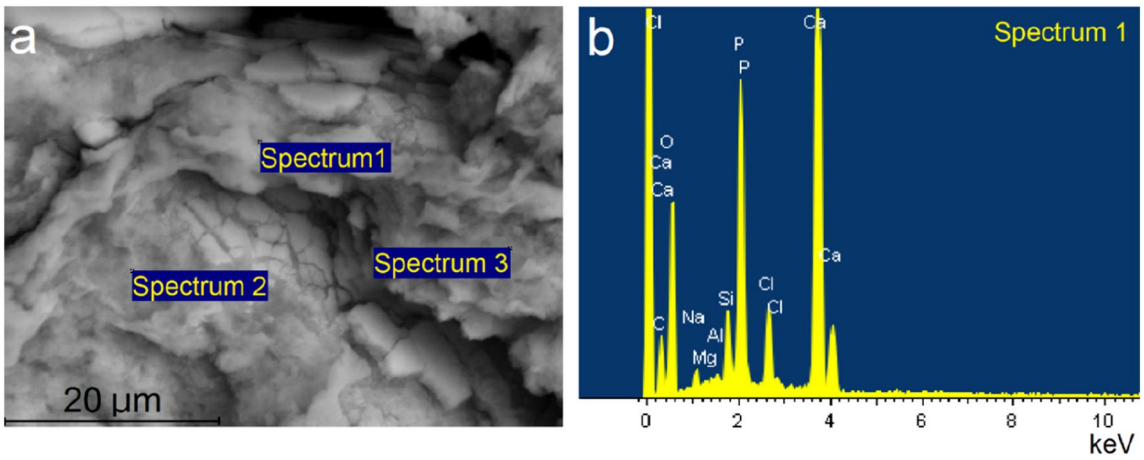

Fig. 2 The SEM images and results of EDS studies of HA–Alg. **a** HA–Alg surface with marked analysis places; **b** corresponding EDS spectra of HA–Alg composite

Table 1 EDS analysis results of HA–Alg composite, wt%

Spectrum	O	Na	Mg	Al	Si	P	Cl	Ca	Sum	Ca/P
Spectrum 1	50.68	1.20	0.25	0.17	2.02	11.40	3.99	28.05	100.00	2.46
Spectrum 2	49.48	1.14	0.35	0.29	2.28	12.93	3.67	29.86	100.00	2.30
Spectrum 3	50.30	1.04	0.42	0.31	2.19	12.63	3.64	29.48	100.00	2.33
max	50.68	1.20	0.42	0.31	2.28	12.93	3.99	29.86		
min	49.48	1.04	0.25	0.17	2.02	11.40	3.64	29.05		

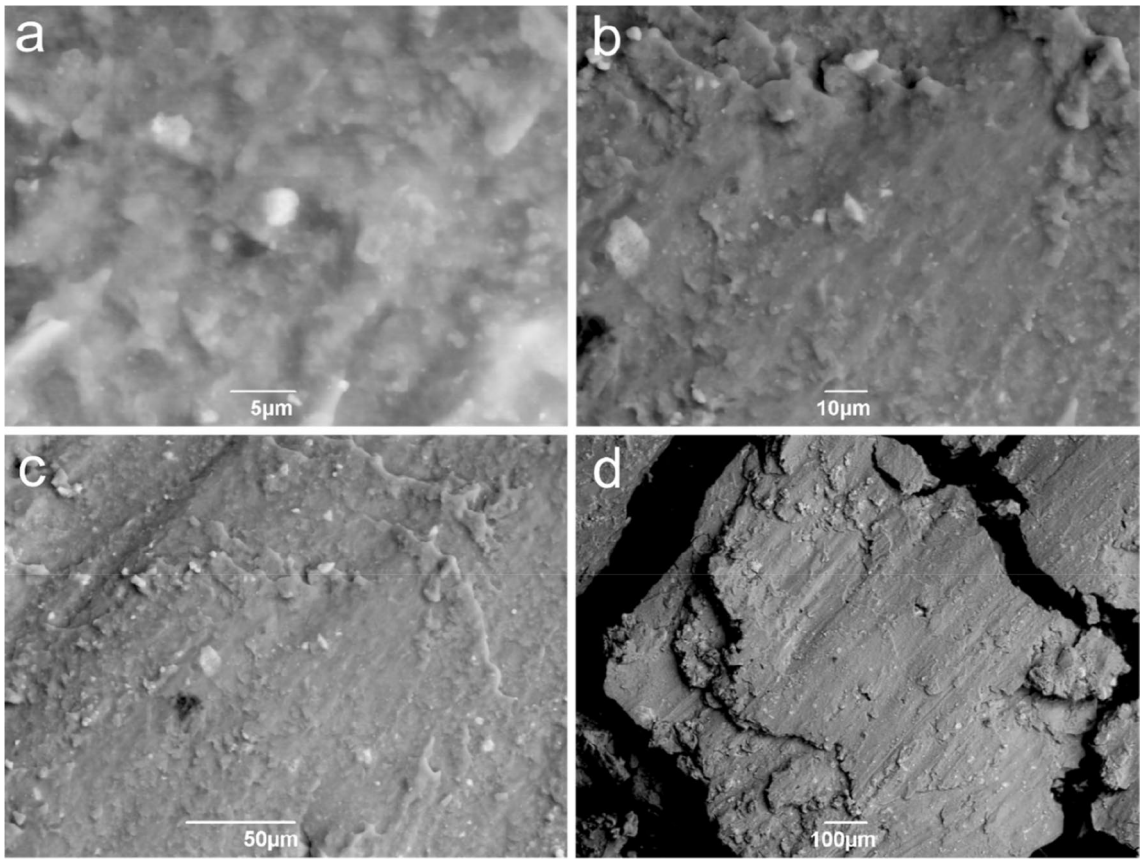

Fig. 3 The SEM image of HA–Fe_3O_4 composite. Magnification: **a** × 3000; **b** × 1000; **c** × 500; **d** × 100

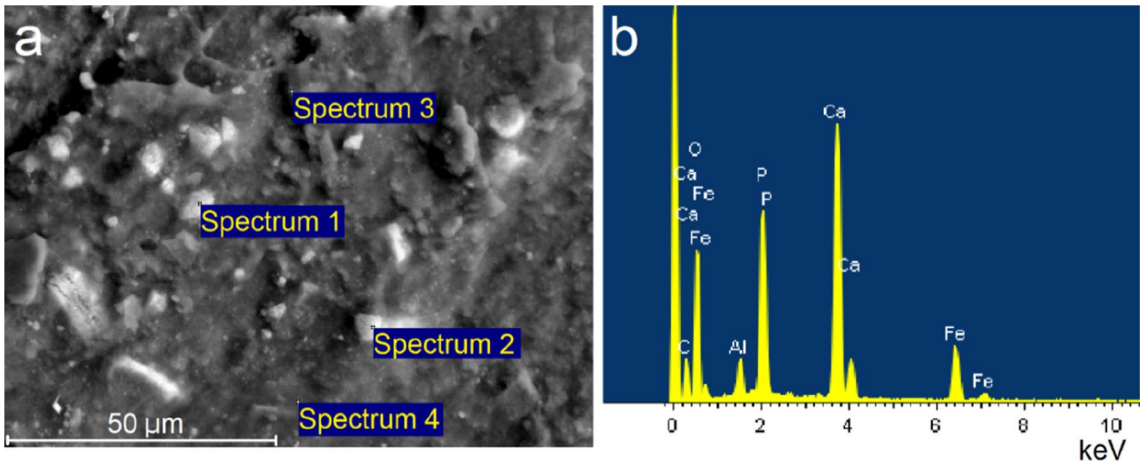

Fig. 4 The SEM images and results of EDS studies of HA–Fe_3O_4. **a** HA–Alg surface with marked analysis places; **b** corresponding EDS spectra of HA–Alg composite

can be seen from the EDAX spectrum presented in Fig. 4b, the O, Al, P, Ca, and Fe elements are presented in the regions. Moreover, the concentration of Fe varies from 3.30 to 12.82 wt%, see Table 2.

Table 2 EDS analysis results of HA–Fe_3O_4 hydrogel, wt%

Spectrum	O	Al	P	Ca	Fe	Sum	Ca/P
Spectrum 1	50.01	1.91	11.83	23.42	12.82	100.00	1.97
Spectrum 2	48.78	2.10	12.17	24.80	12.15	100.00	2.03
Spectrum 3	50.23	1.45	14.39	30.51	3.42	100.00	2.12
Spectrum 4	50.88	1.49	14.58	29.75	3.30	100.00	2.04
Average	49.97	1.74	13.24	27.12	7.92	100.00	2.04
Stand. deviation	0.88	0.32	1.44	3.54	5.28		
Max	50.88	2.10	14.58	30.51	12.82		
Min	48.78	1.45	11.83	23.42	3.30		

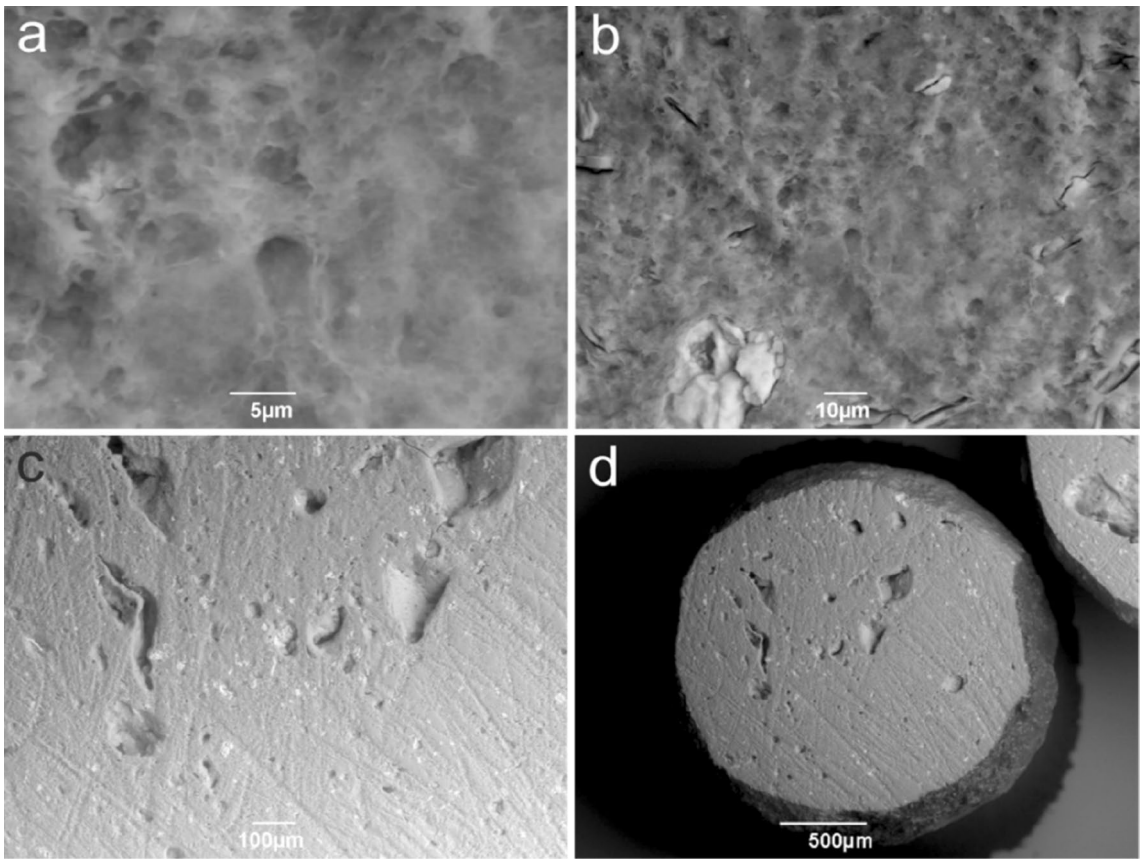

Fig. 5 SEM cross-sectional image of HA–Fe_3O_4–Alg bead. Magnification: **a** × 3000; **b** × 1000; **c** × 100; **d** × 40

The morphology of HA–Fe_3O_4–Alg composite beads is shown in Fig. 5. We conclude that magnetite reduces the homogenization of HA distribution, blocking the formation of lamellae.

The concentration of Fe also varies from 17.70 to 2.22 wt% considerably, Table 3. The Ca/P weight ratio is 2.1, which is slightly lower than stoichiometric ratio of HA (2.15). The absence of hydroxyapatite lamellae formation process, as well as an increased content of Ca and P at the magnetite particle surface (Fig. 6a, spectrum 1 and 2), may indicate an accumulation of hydroxyapatite around magnetite particles by itself.

The following figure shows elements' distribution of HA–Fe_3O_4–Alg composite sample. In elemental contrast, almost all elements, except Fe and O, are evenly distributed (Fig. 7).

3.2 Structure characterization

The XRD investigations were carried out for HA–Fe_3O_4 hydrogel and HA–Fe_3O_4–Alg beads. Since, the same

Table 3 EDS analysis results of HA–Fe_3O_4–Alg beads, wt%

Spectrum	O	Na	Mg	Al	Si	P	Cl	Ca	Fe	Sum	Ca/P
Spectrum 1	46.02	0.92	0.00	0.31	3.47	9.09	3.14	19.34	17.70	100.0	2.13
Spectrum 2	46.21	0.86	0.15	0.23	2.40	9.41	3.29	20.40	17.05	100.0	2.17
Spectrum 3	48.42	0.73	0.26	0.31	2.50	13.06	3.89	28.62	2.22	100.0	2.19
Average	46.88	0.84	0.14	0.28	2.79	10.52	3.44	22.79	12.32	100.0	2.17
Stand. deviation	1.33	0.10	0.13	0.05	0.59	2.21	0.40	5.08	8.76		
Max	48.42	0.92	0.26	0.31	3.47	13.06	3.89	28.62	17.70		
Min	46.02	0.73	0.00	0.23	2.40	9.09	3.14	19.34	2.22		

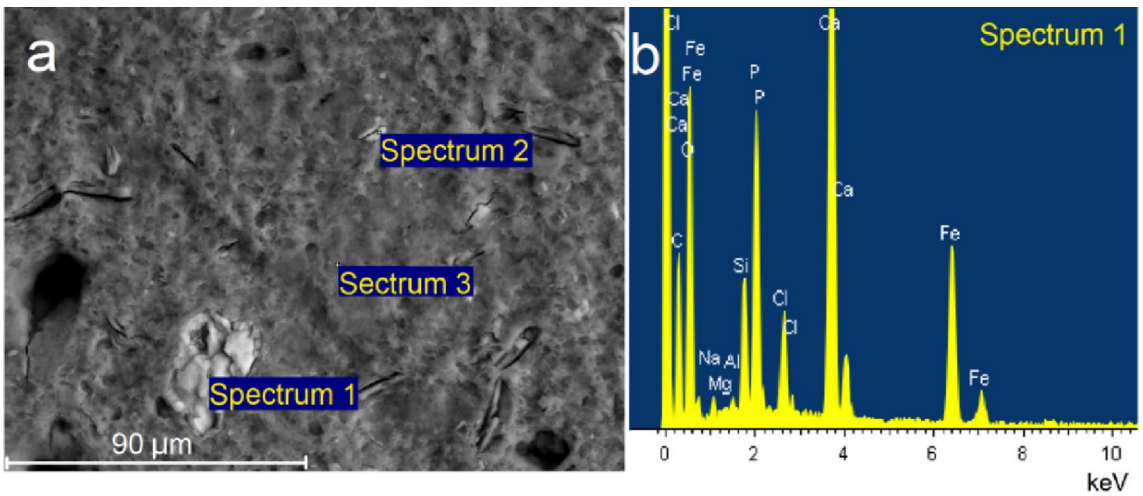

Fig. 6 The SEM images and results of EDS studies of HA–Fe_3O_4–Alg. **a** HA–Fe_3O_4–Alg surface with marked analysis places; **b** corresponding EDS spectra of HA–Fe_3O_4–Alg composite

pre-synthesized HA was applied for the formation of both composite materials, XRD spectra for HA–Fe_3O_4 hydrogel and HA–Fe_3O_4–Alg beads are close (Fig. 8). According to XRD, there are presence of single calcium-deficient HA (JCPDS 45-0905) phase with good crystallinity.

As mentioned above, HA was synthesized under the influence of microwave irradiation. The use of MW (600-W) radiation significantly reduces the time (up to 20 min) of obtaining calcium-deficient hydroxyapatite (cdHA, type B) in the form of a nanopowder, the structure and composition of which are close to biological hydroxyapatite. Importantly, the formation of cdNA nanocrystals under the influence of MW radiation occurs during one stage compared to standard synthesis, which begins with the formation of amorphous calcium phosphate phase (ACP). The main reason for this phenomenon is rapid absorption of radiation energy, which contributes to dehydration of reaction ions Ca^{2+}, OH^- and PO_4^{3-} [30].

Figure 9 presents TEM image of magnetite, obtained according to the method mentioned above (p.2.2.2). The particles' linear dimensions and the results' statistical processing are presented in the form of a histogram.

Studies have shown that the presence of sodium alginate during synthesis leads to a decrease of magnetite nanoparticles size. According to the histogram, about 40% of particles have a size of 8 nm; while, the largest proportion of nanoparticles have a size of 12 nm in polymer-free solution. Small magnetite particles have significant surface energy and there are most effective in terms of antibacterial action [34]. But we must also remember that the reduction in size leads to increased aggregation due to their high specific surface area. Thus, the degree of aggregation of Fe_3O_4 nanoparticles can significantly affect the activity and properties of biocomposites with their content.

In the case of Fe_3O_4 nanoparticles synthesis in the presence of alginate, its hydroxyl groups can generate an interfacial bonding with magnetite nanoparticles and, thus, prevent its growth and agglomeration. The alginate acts as a dispersant and provides the uniform distribution of magnetite nanoparticles within Alg matrix under sonification, during beads forming. Also, Fe_3O_4 nanoparticles in combination with cross-linked Ca^{2+} ions and Alg macromolecules, contribute to enhancement stability of the beads' shape.

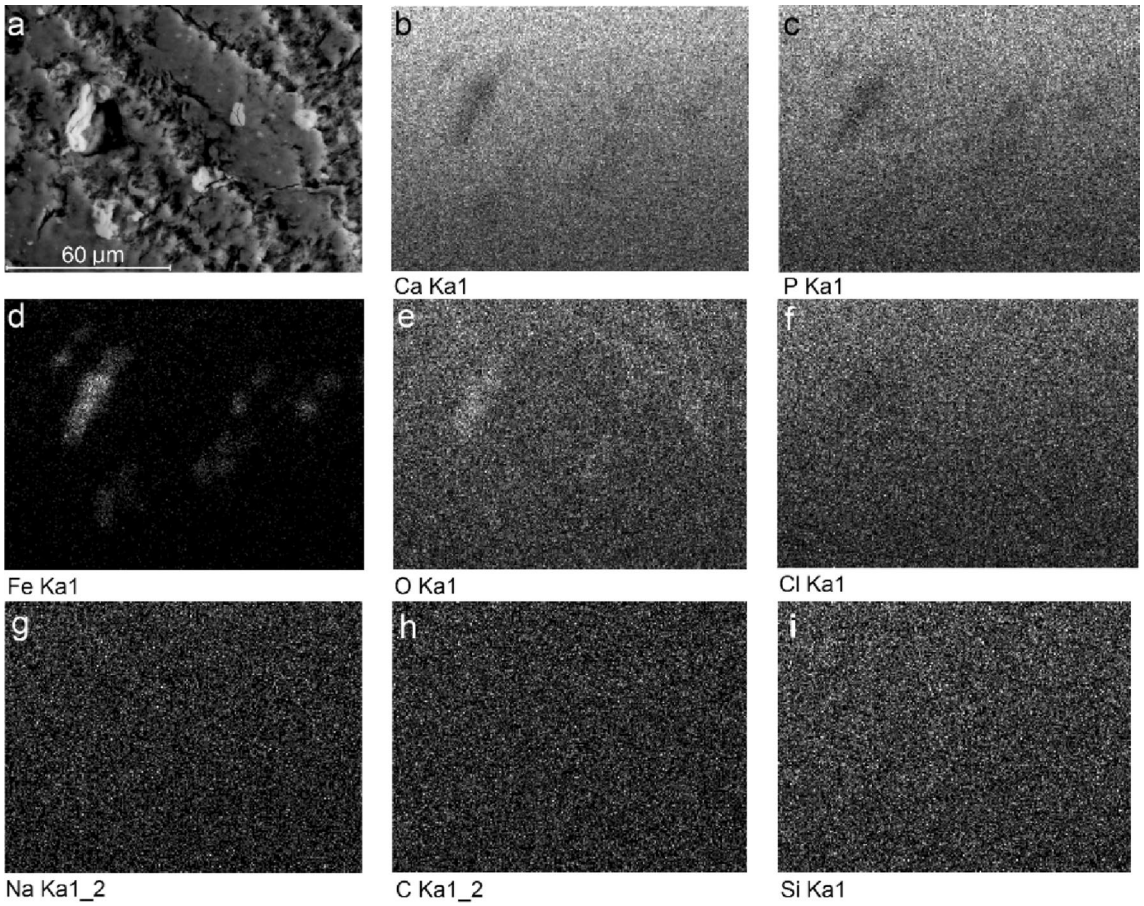

Fig. 7 The SEM images and results of EDS studies of HA–Fe_3O_4–Alg, element maps

It is well known that HA has properties of osteoconductivity and osteoinductivity. Sodium alginate, as it is known, is a nutrient medium for cell proliferation. Particles of magnetite are known to have antimicrobial action and, therefore, may have a negative effect on the proliferation of other cells.

3.3 The study of composite materials on cytotoxicity and biocompatibility

The main premise of tissue engineering is the development of coatings and implants for restore the functions of damaged human tissues. One of the main functions of such scaffold materials is to ensure cells attachment for further cell proliferation and differentiation [35].

Furthermore, they must also ensure the preservation of cells phenotype and viability.

Biocompatibility of composite material in vitro conditions was assessed on viability level, adhesive properties, morphology, proliferation and differentiation of cells.

Cytological examination of the state of cultured fibroblasts (Fig. 10a, b) on the 3rd day in cultures with experimental samples and in the control culture did not reveal any differences. The structural organization of cells testified to their belonging to young fibroblasts. On the 5th day of the cultivation, a significant increase in the cell density was observed.

Cells, which were predominantly mature fibroblasts, retained their phenotype in cultures. The investigation of cytotoxicity was carried out for the samples presented in two aggregate forms—hydrogels and beads. The study of the dead cells number and the total number of cells in cultures was carried out on 3 and 5 days after samples exposure to the culture medium.

The distribution of total number of cells and the number of dead cells did not have a significant difference compared to control culture (Table 4, Fig. 11).

The number of dead cells of control culture after 5 days of exposure was 6.1%; while for the experimental cultures with HA–Fe_3O_4 hydrogel and HA–Fe_3O_4–Alg beads, these values were 5.4% and 12.9%, respectively. It does not exceed the permissible limits for primary crops. Attention is drawn to the fact that the highest number of dead cells (12.9%) was recorded for the sample with magnetite HA–Fe_3O_4–Alg beads. Cell growth over the period from

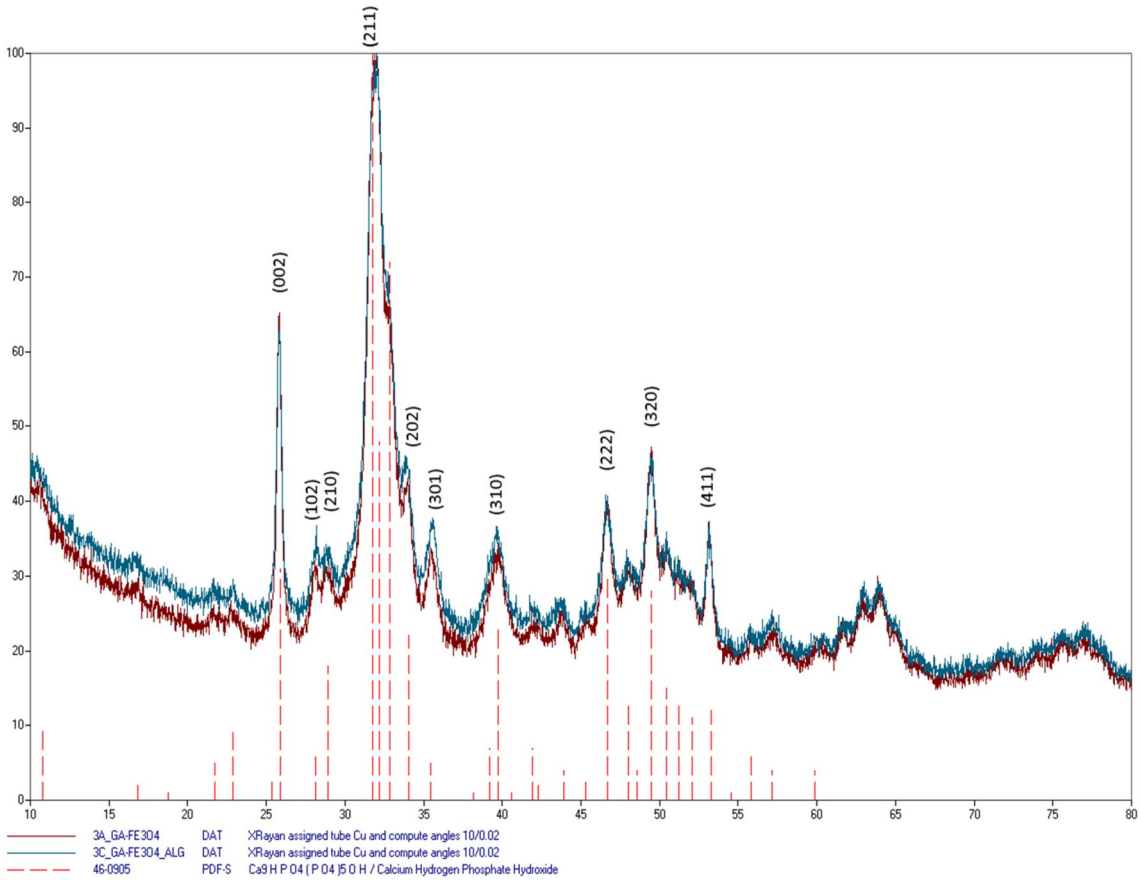

Fig. 8 Diffraction patterns of HA–Fe_3O_4 hydrogel and HA–Fe_3O_4–Alg beads samples

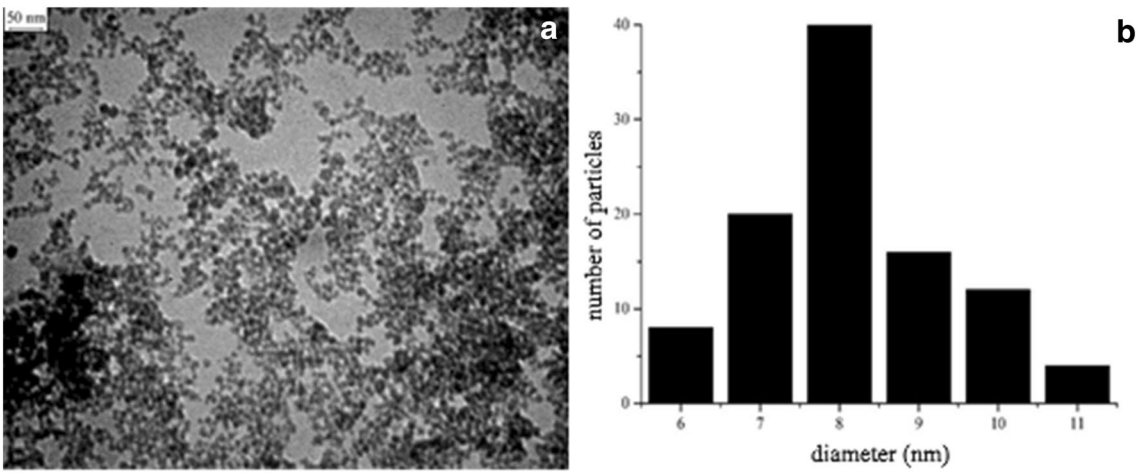

Fig. 9 TEM image of magnetite nanoparticles, obtained in the presence of alginate (**a**) and histogram of their size distribution (**b**)

3 to 5 days for this sample is also the smallest (57.3%) as compared to control and hydrogel samples. Experimental data show that the behavior of osteoblasts and fibroblasts depends on the sample structure and changes during the transition from hydrogel to beads. Thus, in the case of HA–Fe_3O_4 hydrogel, a smaller number of dead cells is characteristic. Moreover, that samples have higher degree of cells proliferation in the period from 3 to 5 days compared to HA–Fe_3O_4–Alg beads. This fact can be explained as follows: hydrogel has more developed surface, which

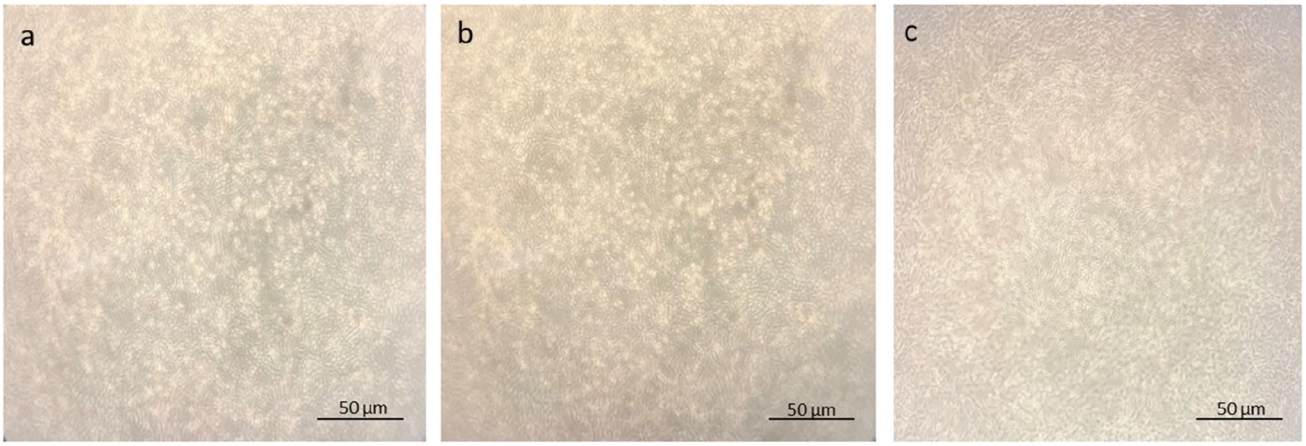

Fig. 10 Morphology of fibroblast cells **a** for 3 days; **b** for 5th day of cultivation with materials HA–Fe_3O_4 hydrogel and HA–Fe_3O_4–Alg beads (×50)

Table 4 Dynamics of cells survival and cells proliferation in contact with experimental samples ($p \leq 0.05$)

Sample	3 days		5 days		The increase in the total number of cells for 2 days, in %
	Total number of cells	Number of dead cells, incl. in %	Total number of cells	Number of dead cells, incl. in %	
Culture (control)	1.98×10^4	6.93×10^2 3.5%	3.21×10^4	1.96×10^3 6.1%	62.1
HA–Alg beads	1.81×10^4	1.41×10^3 7.8%	2.96×10^4	1.09×10^3 10.9%	63.5
HA–Fe_3O_4 hydrogel	1.83×10^4	7.69×10^2 4.2%	2.95×10^4	1.59×10^3 5.4%	61.2
HA–Fe_3O_4–Alg beads	1.92×10^4	1.94×10^3 10.1%	3.02×10^4	3.90×10^3 12.9%	57.3

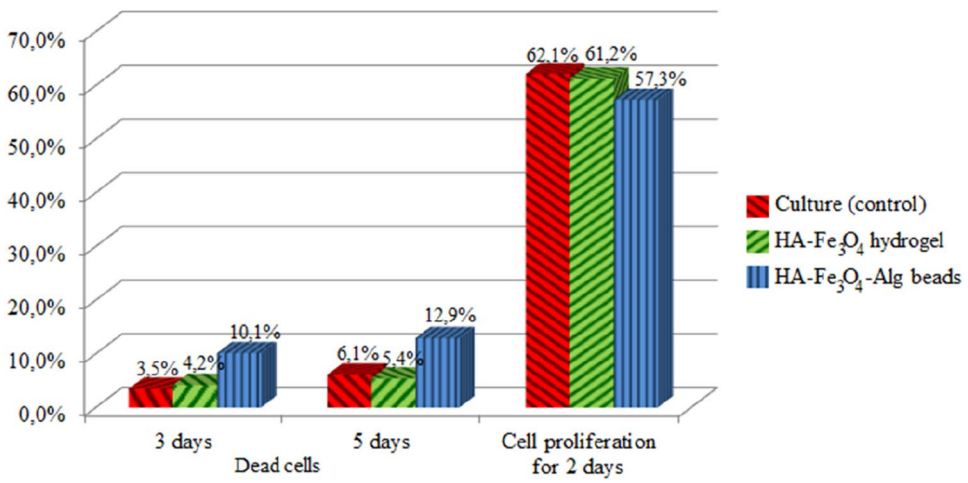

Fig. 11 Comparative characteristics of the influence of experimental samples on the cells behavior in the nutrient medium

implies a higher degree of contact between hydroxyapatite particles and cells. Therefore, HA contributes to cell survival and their proliferation. On the other hand, macromolecules of sodium alginate, as it is known, are a nutrient medium for cell proliferation. In the case of beads, the contact of cells with HA occurs only on the surface of the beads, which reduces the survival rate. It is obvious that the Fe_3O_4 particles also influence the behavior of fibroblasts.

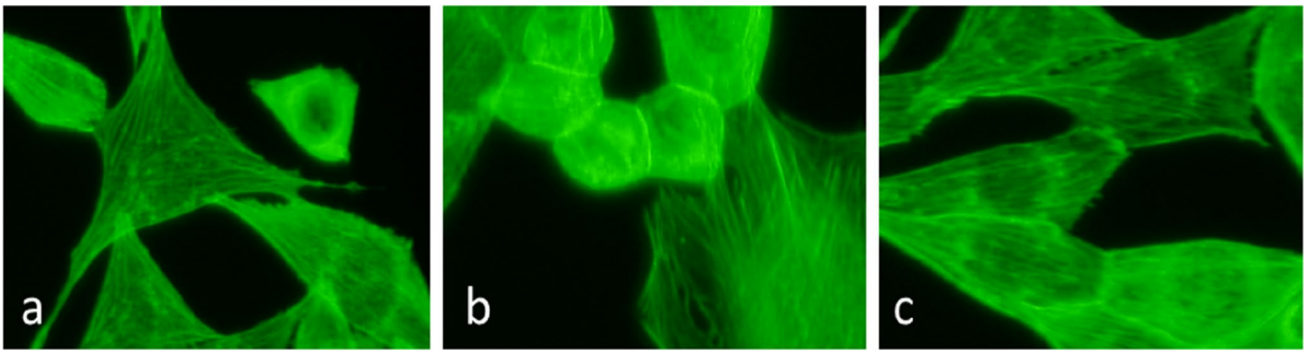

Fig. 12 Fluorescent images of NIH-3T3 cells cultured with experimental samples: **a** control; **b** HA–Fe_3O_4 hydrogel; **c** HA–Alg–Fe_3O_4

Magnetite-containing samples demonstrate a lower degree of proliferation compared to magnetite-free HA–Alg beads. For this sample, that was also used in experiment, the number of dead cells after 5 days of exposure was 10.9%. It should be noted that these data are not above the limit, used for primary crops. Furthermore, the growth of cells between the period from 3 to 5 days was 63.5% which is the highest as compared to the results of other samples.

Only cdHA and Alg have a positive (or neutral) effect on cell proliferation. Magnetite performs a therapeutic function (for example, in the method of hyperthermia in the treatment of bone tumours) and has a certain degree of toxicity, slightly reducing the degree of proliferation. That is why we conducted a thorough study of the cytotoxicity of the created three-component biomaterial.

Thereby, the applied content of magnetite particles (1% to HA dry powder) does not show a negative effect on the cells.

Adhesive and proliferative properties of the cells were assessed by fluorescence microscopy (Fig. 12). To visualize cells, they were pre-stained with fluorogenic dye DHR-123 (provides green fluorescence in metabolically active cells).

Fibroblasts growing in a control medium after 48 h had a typical spindle-shape morphology, formed a number of pseudopodia and covered the bottom of the plate wells. However, fibroblasts grown on cellulose membranes had round morphology after 2 days of cultivation (Fig. 12a–c). The reason for the dissimilarities in the cell phenotype on the bottom of plastic plates and HA–Fe_3O_4 hydrogel and HA–Alg–Fe_3O_4 surface is related to the difference in substrate stiffness. It was shown that cells generate a greater traction force and develop a broader and flatter morphology on stiff substrates than they do on soft but equally adhesive substrates. However, when fibroblast cells become confluent and make contact using their internal signals leading to cell spreading and proliferation, the stiffness of the substrate no longer affects their morphology [19, 36, 37].

It should be highlighted that the fibroblasts that were growing in a medium containing HA–Alg after 48 h showed the results as having spindle-shape structure with the good bottom coverage also, as in the control one. Cells were characterized by normal morphology and showed good adhesive ability. The green fluorescence of cultivated cells evidenced its metabolic activity.

4 Conclusions

In this work, Fe_3O_4-loaded hydroxyapatite-based composite biomaterials were synthesized in the form of hydrogel and beads. The polymer presence during the synthesis reduces an average size of magnetite nanoparticles. About 40% of particles have a size of 8 nm according to the TEM data and histogram of size distribution. SEM pictures demonstrate the porous structure of the beads, representing calcium alginate matrix with immobilized particles of HA and magnetite. Cytological characteristics of fibroblasts in cultures were studied. The increase in the total number of cells in cultures, the way of their arrangements, the number of destructively modified and dead cells confirm the steady growth of fibroblasts on the 5th day of experiment in both the control and experimental series of samples. The presence of magnetite applied samples in the nutrient medium did not effect on cells viability. This is the evidence that tested composites are biocompatible. Although in vitro results cannot be extrapolated in vivo, they may provide very valuable information for tissue engineering.

Funding Funding was provided by Ministry of Education and Science of the Republic of Kazakhstan (Grant no 0117PK00047).

References

1. R. Agarwal, A.J. García, Biomaterial strategies for engineering implants for enhanced osseointegration and bone repair. Adv. Drug Deliv. Rev. **94**, 53–62 (2015). https://doi.org/10.1016/j.addr.2015.03.013
2. W. Suchanek, M. Yoshimura, Processing and properties of hydroxyapatite-based biomaterials for use as hard tissue replacement implants. J. Mater. Res. **13**(01), 94–117 (1998). https://doi.org/10.1557/JMR.1998.0015
3. T. Gong, J. Xie, J. Liao, T. Zhang, S. Lin, Y. Lin, Nanomaterials and bone regeneration. Bone Res. (2015). https://doi.org/10.1038/boneres.2015.29
4. A.E. Jakus, R.N. Shah, Multi and mixed 3D-printing of graphene-hydroxyapatite hybrid materials for complex tissue engineering. J. Biomed. Mater. Res. Part A. **105**(1), 274–283 (2017). https://doi.org/10.1002/jbm.a.35684
5. A. Turlybekuly, A. Sagidugumar, Y. Otarov et al., Bacterial cellulose/hydroxyapatite printed scaffolds for bone engineering. Nanomater. Biomed. Appl. Biosens. (2020). https://doi.org/10.1007/978-981-15-3996-1_1
6. J. Venkatesan, I. Bhatnagar, P. Manivasagan, K.-H. Kang, S.-K. Kim, Alginate composites for bone tissue engineering: a review. Int. J. Biol. Macromol. **72**, 269–281 (2015). https://doi.org/10.1016/j.ijbiomac.2014.07.008
7. K.Y. Lee, D.J. Mooney, Alginate: properties and biomedical applications. Prog. Polym. Sci. **37**(1), 106–126 (2012). https://doi.org/10.1016/j.progpolymsci.2011.06.003
8. J. Sun, H. Tan, Alginate-based biomaterials for regenerative medicine applications. Materials (Basel) **6**(4), 1285–1309 (2013). https://doi.org/10.3390/ma6041285
9. F.-Y. Hsu, R.-C. Weng, H.-M. Lin et al., A biomimetic extracellular matrix composed of mesoporous bioactive glass as a bone graft material. Microporous Mesoporous Mater. **212**, 56–65 (2015). https://doi.org/10.1016/j.micromeso.2015.03.027
10. A. Hajinasab, S. Saber-Samandari, S. Ahmadi, K. Alamara, Preparation and characterization of a biocompatible magnetic scaffold for biomedical engineering. Mater. Chem. Phys. (2018). https://doi.org/10.1016/j.matchemphys.2017.10.080
11. E. Díaz, M. Valle, S. Ribeiro, S. Lanceros-Mendez, J. Barandiarán, Development of magnetically active scaffolds for bone regeneration. Nanomaterials **8**(9), 678 (2018). https://doi.org/10.3390/nano8090678
12. F. Márquez, G.M. Herrera, T. Campo et al., Preparation of hollow magnetite microspheres and their applications as drugs carriers. Nanoscale Res. Lett. **7**(1), 210 (2012). https://doi.org/10.1186/1556-276X-7-210
13. V.F. Cardoso, A. Francesko, C. Ribeiro, M. Bañobre-López, P. Martins, S. Lanceros-Mendez, Advances in magnetic nanoparticles for biomedical applications. Adv. Healthc. Mater. (2018). https://doi.org/10.1002/adhm.201700845
14. M. Świętek, W. Tokarz, J. Tarasiuk, S. Wroński, M.B. Łazewicz, Magnetic polymer nanocomposite for medical application. Acta Phys. Pol. A. (2014). https://doi.org/10.12693/APhysPolA.125.891
15. V. Mailänder, K. Landfester, Interaction of nanoparticles with cells. Biomacromol **10**(9), 2379–2400 (2009). https://doi.org/10.1021/bm900266r
16. V. Torchilin, Multifunctional nanocarriers. Adv. Drug Deliv. Rev. **58**(14), 1532–1555 (2006). https://doi.org/10.1016/j.addr.2006.09.009
17. K. Ulbrich, K. Holá, V. Šubr, A. Bakandritsos, J. Tuček, R. Zbořil, Targeted drug delivery with polymers and magnetic nanoparticles: covalent and noncovalent approaches, release control, and clinical studies. Chem. Rev. **116**(9), 5338–5431 (2016). https://doi.org/10.1021/acs.chemrev.5b00589
18. X. Hu, G. Liu, Y. Li, X. Wang, S. Liu, Cell-penetrating hyperbranched polyprodrug amphiphiles for synergistic reductive milieu-triggered drug release and enhanced magnetic resonance signals. J. Am. Chem. Soc. **137**(1), 362–368 (2015). https://doi.org/10.1021/ja5105848
19. X. Tian, L. Zhang, M. Yang et al., Functional magnetic hybrid nanomaterials for biomedical diagnosis and treatment. Wiley Interdiscip. Rev. Nanomed. Nanobiotechnol. **10**(1), e1476 (2018). https://doi.org/10.1002/wnan.1476
20. J. Lin, M. Wang, H. Hu et al., Multimodal-imaging-guided cancer phototherapy by versatile biomimetic theranostics with UV and γ-irradiation protection. Adv. Mater. **28**(17), 3273–3279 (2016). https://doi.org/10.1002/adma.201505700
21. H. Arami, E. Teeman, A. Troksa et al., Tomographic magnetic particle imaging of cancer targeted nanoparticles. Nanoscale **9**(47), 18723–18730 (2017). https://doi.org/10.1039/C7NR05502A
22. N.M. Sundaram, S. Murugesan, Preparation and characterization of an iron oxide-hydroxyapatite nanocomposite for potential bone cancer therapy. Int. J. Nanomed. (2015). https://doi.org/10.2147/IJN.S79985
23. J. Yang, S. Park, H. Yoon, Y. Huh, S. Haam, Preparation of poly ε-caprolactone nanoparticles containing magnetite for magnetic drug carrier. Int. J. Pharm. **324**(2), 185–190 (2006). https://doi.org/10.1016/j.ijpharm.2006.06.029
24. Y. Zhao, T. Fan, J. Chen et al., Magnetic bioinspired micro/nanostructured composite scaffold for bone regeneration. Colloids Surf. B Biointerfaces **174**, 70–79 (2019). https://doi.org/10.1016/j.colsurfb.2018.11.003
25. A. Hervault, N.T.K. Thanh, Magnetic nanoparticle-based therapeutic agents for thermo-chemotherapy treatment of cancer. Nanoscale **6**(20), 11553–11573 (2014). https://doi.org/10.1039/C4NR03482A
26. M.K. Lima-Tenório, E.A. Gómez Pineda, N.M. Ahmad, H. Fessi, A. Elaissari, Magnetic nanoparticles: in vivo cancer diagnosis and therapy. Int. J. Pharm. **493**(1–2), 313–327 (2015). https://doi.org/10.1016/j.ijpharm.2015.07.059
27. S.V. Dorozhkin, Calcium orthophosphates (CaPO4): occurrence and properties. Prog. Biomater. **5**(1), 9–70 (2016). https://doi.org/10.1007/s40204-015-0045-z
28. E.A. Périgo, G. Hemery, O. Sandre et al., Fundamentals and advances in magnetic hyperthermia. Appl. Phys. Rev. **2**(4), 041302 (2015). https://doi.org/10.1063/1.4935688
29. A.S. Stanislavov, A.A. Yanovska, V.N. Kuznetsov, L.B. Sukhodub, L.F. Sukhodub, The comparison of magnetite nanospheres formation in polysaccharide covers by various ways of syntheses. J Nanoelectron Phys. **7**(2), 02009 (2015)
30. A.S. Stanislavov, L.F. Sukhodub, L.B. Sukhodub, V.N. Kuznetsov, K.L. Bychkov, M.I. Kravchenko, Structural features of hydroxyapatite and carbonated apatite formed under the influence of ultrasound and microwave radiation and their effect on the bioactivity of the nanomaterials. Ultrason. Sonochem. (2018). https://doi.org/10.1016/j.ultsonch.2017.11.011
31. A. Turlybekuly, A.D. Pogrebnjak, L.F. Sukhodub et al., Synthesis, characterization, in vitro biocompatibility and antibacterial properties study of nanocomposite materials based on hydroxyapatite-biphasic ZnO micro- and nanoparticles embedded in Alginate matrix. Mater. Sci. Eng. C (2019). https://doi.org/10.1016/j.msec.2019.109965
32. A. Pogrebnjak, L. Sukhodub, L. Sukhodub et al., Composite material with nanoscale architecture based on bioapatite, sodium alginate and ZnO microparticles. Ceram. Int.

45(6), 7504–7514 (2019). https://doi.org/10.1016/j.ceramint.2019.01.043
33. A.D. Pogrebnjak, L.F. Sukhodub, L. Sukhodub, O.V. Bondar, A. Turlybekuly, ZnO doped nanosized composite material based on hydroxyapatite and sodium alginate matrix. Adv. Thin Film Nanostruct. Mater. Coat. (2019). https://doi.org/10.1007/978-981-13-6133-3_35
34. S. Stankic, S. Suman, F. Haque, J. Vidic, Pure and multi metal oxide nanoparticles: synthesis, antibacterial and cytotoxic properties. J. Nanobiotechnol. **14**(1), 73 (2016). https://doi.org/10.1186/s12951-016-0225-6
35. R.D. Sinclair, T.J. Ryan, Proteolytic enzymes in wound healing: the role of enzymatic debridement. Australas. J. Dermatol. **35**(1), 35–41 (1994). https://doi.org/10.1111/j.1440-0960.1994.tb01799.x
36. A.D. Pogrebnjak, C.-H. Kong, R.F. Webster et al., Antibacterial effect of Au implantation in ductile nanocomposite multilayer (TiAlSiY)N/CrN Coatings. ACS Appl. Mater. Interfaces **11**(51), 48540–48550 (2019). https://doi.org/10.1021/acsami.9b16328
37. A. Shypylenko, A.V. Pshyk, B. Grześkowiak et al., Effect of ion implantation on the physical and mechanical properties of Ti–Si–N multifunctional coatings for biomedical applications. Mater. Des. **110**, 821–829 (2016). https://doi.org/10.1016/j.matdes.2016.08.050